INORGANIC CHEMISTRY FRONTIERS

RESEARCH ARTICLE

View Article Online
View Journal | View Issue

Cite this: *Inorg. Chem. Front.*, 2023, **10**, 3699

Novel COF@Ti–MOF hybrid photocatalysts enabling enhanced photocatalytic CO_2 reduction in a gas–solid system without additives†

Rui-Gang Yang,[a] Yao-Mei Fu,[b] Xing Meng,[a] Li Xue,[a] Zhen Zhou,[a] Yu-Ou He,[a] Jian-Xin Qu,[a] Hai-Ning Wang *[a] and Zhong-Min Su[b,c]

Received 3rd February 2023,
Accepted 15th May 2023

DOI: 10.1039/d3qi00217a

rsc.li/frontiers-inorganic

With the increasing global energy demand and environmental problems, the photoreduction of CO_2 into valuable chemical materials is considered to be an ideal way to recycle carbon resources. Naturally, the design and synthesis of efficient photocatalysts used for the photocatalytic reduction of CO_2 still face great challenges. Herein, a series of stable hybrid photocatalysts **TpPa@IEF** has been produced by integrating the two-dimensional covalent organic framework **TpPa-1** with the Ti-based metal–organic framework **IEF-11**. The photocatalytic performance of **TpPa@IEF** has been evaluated *via* gas–solid reaction mode under visible light as well as no sacrificial agents and photosensitizers. The experimental results show that **TpPa@IEF** exhibits excellent photocatalytic activity in pure and dilute CO_2 (10%) environments. The introduction of **IEF-11** has resulted in a significant improvement in photocatalytic performance; **TpPa@IEF** achieved a great CO generation rate of 78.87 μmol g^{-1} h^{-1} in pure CO_2, notably, and obtained another excellent CO generation rate of 116.47 μmol g^{-1} h^{-1} in dilute CO_2 (10%), which are 3.63 and 4.93 times higher than that of **TpPa-1**, respectively. The excellent photocatalytic performance of **TpPa@IEF** hybrids stems from the high charge separation efficiency and CO_2 capture ability, as well as the abundant catalytic active sites. The preparation of **TpPa@IEF** hybrid materials presents a novel perspective for the design and synthesis of efficient photocatalysts.

Introduction

The excessive consumption of fossil fuels leads to the increasing concentration of carbon dioxide (CO_2) in the atmosphere, which leads to a series of environmental problems, for example, the greenhouse effect. Therefore, developing new technologies for the enrichment and conversion of CO_2 and realizing closed-loop utilization of CO_2 can alleviate the energy and environmental crisis. The strategies for the conversion of CO_2 include photochemical conversion,[1,2] biological conversion,[3,4] CO_2 hydroconversion[5] and electrochemical conversion.[6,7] Compared with other methods, the reduction of CO_2 into renewable fuels using photocatalysts has many advantages and is considered to be an environmentally friendly and efficient method to realize the carbon cycle. Therefore, there is an urgent need to develop an efficient photocatalyst that can capture visible light and effectively suppress the recombination of photogenerated carriers, converting CO_2 into chemical materials effectively.

As a booming family of porous materials, covalent organic frameworks (COFs) composed of organic molecules assembled through covalent bonds have been the subject of wide-ranging research in various areas such as catalysis, gas storage, sensing, *etc.*[8,9] With long-range ordered structures, designable band gaps, and large surface areas, COFs have appeared as a new family of photoactive materials for photocatalytic reduction of CO_2.[10] In addition, most COFs have extensive light trapping in the visible region due to the absorption properties of functional groups and large conjugation systems. Based on these advantages, Lostch *et al.*[11] employed TFPT–COF as a photocatalytic platform to achieve an efficient catalytic activity for the first time. Although COFs show many advantages in the photocatalysis field,[12] severe charge carrier

[a]*School of Chemistry and Chemical Engineering, Shandong University of Technology, Zibo 255049, People's Republic of China. E-mail: wanghn913@foxmail.com*
[b]*Shandong Engineering Research Center of Green and High-value Marine Fine Chemical, Weifang University of Science and Technology, Shouguang, 262700, China*
[c]*School of Chemistry and Environmental Engineering, Changchun University of Science and Technology, Changchun, 130022, China*

†Electronic supplementary information (ESI) available: Materials and methods, experimental details including synthesis, experimental procedure, supporting data, and FTIR spectra of photocatalysts, PXRD patterns, CO_2 adsorption, Mott–Schottky plots, XPS spectrum, PL spectra, time-yield graph and table of CO on TpPa@IEF-X, UV-visible absorption spectrum. See DOI: https://doi.org/10.1039/d3qi00217a

recombination remains the main obstacle to further optimizing their photocatalytic performance. Therefore, various approaches, including ligand functionalization, metal doping, and heterostructure construction, have been developed to address the above problem.[13–15] Until now, there have been several examples of COF-based photocatalysts, such as Au/TAPB–DMTP–COF, α-Fe_2O_3/TpPa–2-COF and MoS_2/TpPa–1-COF, which could effectively solve the problem of low carrier utilization efficiency, resulting in enhanced photocatalytic activity.[16–18] The valuable achievements provide an important idea for the design of new composite catalysts.

Metal–organic frameworks (MOFs), which are another class of crystalline porous materials, exhibit the advantages of large surfaces, bountiful active catalytic sites, and tunable and designed structures.[19] Up to now, some famous frameworks such as the UIO, PCN, ZIFs and MIL series have been widely studied and are extensively applied in the fields of gas adsorption and separation,[20,21] energy storage,[22,23] drug transport[24,25] and catalysis,[26] especially in the field of photocatalysis.[27–30] Among the reported MOFs, the inherent advantages of Ti-based MOFs, such as high chemical stability, good photocatalytic activity, and being clean and pollution-free, are widely studied and applied.[31,32] However, there are a few reports on Ti-based MOFs explored in the area of photocatalytic reduction of CO_2.[33]

The reported works on COF-based photocatalysts inspire us to develop new hybrid photocatalysts. MOFs have been demonstrated to be able to form heterojunctions with COFs well,[34,35] and the photocatalytic performances of the generated hybrid materials suppress those of each monomer. Due to their advantages of large surface areas, available porosity and sufficient active sites, as well as their good visible light trapping ability, MOFs and COFs can be used as excellent substitutes for building hybrid photocatalysts. Therefore, **IEF-11** as a Ti-based MOF with abundant catalytic active sites and good electron transport ability and **TpPa-1** as a Schiff base COF with good visible light capture ability are selected to construct hybrid photocatalysts to achieve great photocatalytic performances. Moreover, **IEF-11**[36] and **TpPa-1**[37] have good thermal and chemical stability, which is very beneficial for building a stable photocatalyst.

Based on this background, a class of heterostructured hybrid photocatalysts **TpPa@IEF** based on 3D Ti-based MOF **IEF-11** and 2D COF **TpPa-1** have been successfully proposed in this work, which have a core–shell structure with **TpPa-1** as the core and **IEF-11** as the shell and exhibit great chemical stability. Their photocatalytic performances towards CO_2 have been evaluated driven by visible light under both pure CO_2 and low CO_2 concentration (10%). These heterogeneous photocatalysts, **TpPa@IEF**, are able to achieve CO generation rates of 78.87 μmol g^{-1} h^{-1} and 116.47 μmol g^{-1} h^{-1} in pure CO_2 and 10% CO_2 environments, respectively. Furthermore, a series of characterization studies demonstrates that excellent photocatalytic performance is ascribed to the high charge separation and transfer efficiency and CO_2 capture ability, as well as the abundant catalytic active sites.

Experimental section

The chemical reagents and solvents used in this work are commercially available and were used directly. They are listed in the ESI.† The detailed synthesis process, photochemical test methods and photocatalytic performance tests of all materials are given in the ESI.†

Results and discussion

Herein, a series of hybrid photocatalytic materials based on **TpPa-1** and **IEF-11** were designed and synthesized with the help of the solvothermal method (Scheme 1). 2D COF **TpPa-1** was pre-synthesized through the classical Schiff base reaction. Then, the as-synthesized **TpPa-1** was placed in the mixed system containing titanium isopropoxide and 3,4-dihydroxycyclobut-3-ene-1,2-dione, which were heated in an oven, in order to obtain the target hybrid photocatalysts **TpPa@IEF**. The obtained hybrid photocatalytic materials were named **TpPa@IEF-*X*** (*X* is 50, 100 and 150) according to the mass of **TpPa-1** used.

The chemical structure and the purity of the as-synthesized samples were evaluated *via* powder X-ray diffraction (PXRD) analysis. The PXRD pattern of the **IEF-11** displays real evidence, consistent with the corresponding simulation (Fig. 1a), demonstrating the successful construction of **IEF-11**. All the diffraction peaks of **TpPa@IEF-*X*** are similar to those of **IEF-11** and **TpPa-1** in the PXRD patterns, indicating that the successful integration of **IEF-11** and **TpPa-1** does not affect their structures. Meanwhile, the as-synthesized **TpPa@IEF-150** was selected to demonstrate the chemical stability of the prepared photocatalysts. The samples were immersed in different pH solutions for 24 h, and then, the obtained samples were subjected to PXRD and FT-IR measurements. The test results certify the great chemical stability of the obtained composite photocatalysts (Fig. S1 and S2†). It should be mentioned that the XPS measurements of **TpPa@IEF-150** after treatment with different pH solutions have demonstrated that the elemental

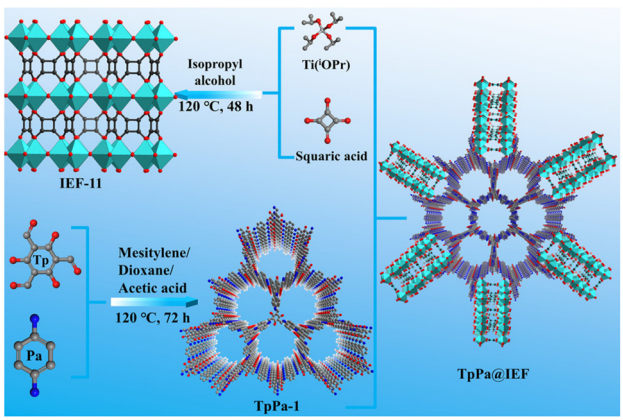

Scheme 1 The schematic diagram of **TpPa@IEF-*X***.

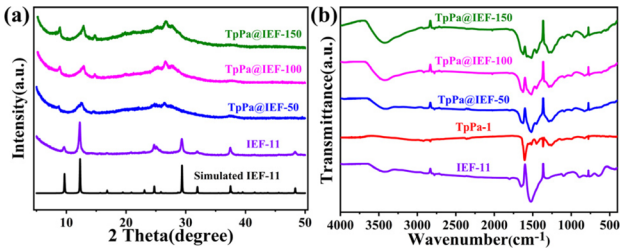

Fig. 1 (a) The PXRD patterns of **IEF-11** and **TpPa@IEF-*X***, and (b) the FT-IR spectra of **TpPa-1**, **IEF-11** and **TpPa@IEF-*X***.

valence states and binding energy magnitudes remain unchanged (Fig. S3–S7†), and the SEM images of **TpPa@IEF-150** after treatment in different pH solutions further demonstrate the structural stability of the material (Fig. S8–S10†). Moreover, the thermogravimetric analysis shows that the samples are capable of maintaining good thermal stability until 300 °C (Fig. S11†).

Fourier transform infrared (FT-IR) spectroscopic analysis was employed to reveal the characteristic chemical bonds of the prepared samples, which was used to confirm the structure of the composite photocatalysts. Fig. 1b shows that the characteristic absorption peak at 640 cm^{-1} belongs to the stretching convulsion of the Ti–O bonds in **IEF-11**.[36] The strong characteristic peaks at 1521 cm^{-1} and 1251 cm^{-1} are attributed to the stretching vibrations of the C=C bond and the β-ketamine bond C–N, respectively.[38] The appearance of the characteristic peak at 1632 cm^{-1} is due to the vibration of the C=O bonds of the 3,4-dihydroxycyclobut-3-ene-1,2-dione and Tp. The FT-IR spectra demonstrate that **TpPa-1** and **IEF-11** have been successfully synthesized and the vibrations of the characteristic peaks of **TpPa-1** and **IEF-11** can be shown in the hybrid material.

The apparent morphology of the as-synthesized samples is observed by the scanning electron microscopy (SEM) characterization (Fig. 2a–d). The SEM image shows that the morphology of **IEF-11** exhibits a regular structure of hexagonal prisms, whose sizes are less than 100 nm. In the hybrid photocatalysts **TpPa@IEF-*X***, **IEF-11** grows on the surface of **TpPa-1**, where **IEF-11** particles become smaller and more irregular as the mass of **TpPa-1** increases. In **TpPa@IEF-50** and **TpPa@IEF-100**, the particles of **IEF-11** grow on the surface of **TpPa-1** thickly, while **IEF-11** particles are thinly distributed on the surface of **TpPa-1** in **TpPa@IEF-150**. The difference in the surface morphology of **TpPa@IEF-*X*** may have an explicit effect on the photocatalytic CO_2 reduction. The TEM images show that **TpPa-1** has a petal-like structure with a smooth surface. Therefore, the images of **TpPa@IEF-*X*** reveal smaller **IEF-11** particles covering the surface of the rod-like structure from **TpPa-1**, resulting in a rough and irregular surface, compared to that of **TpPa-1**, demonstrating that **IEF-11** is successfully distributed at the surface of **TpPa-1**. In a word, **TpPa@IEF-*X*** exhibit a core–shell structure, where **TpPa-1** serves as the core and **IEF-11** as the shell.

The chemical state of each element in **TpPa@IEF-150** has been further investigated by X-ray photoelectron spectroscopy

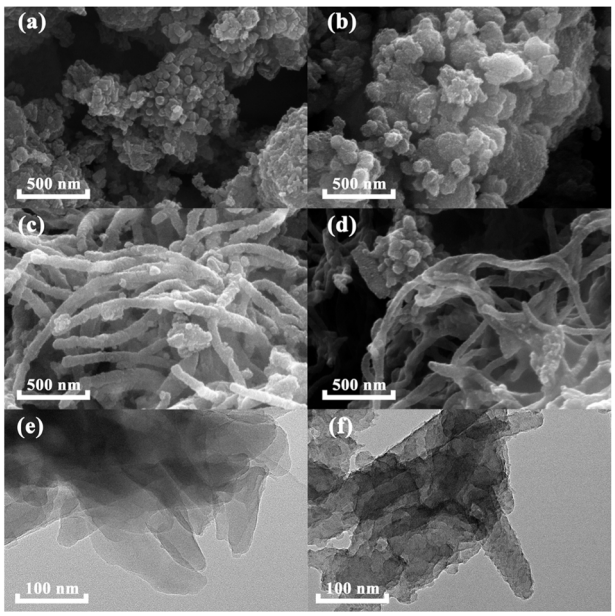

Fig. 2 SEM images of (a) **IEF-11**, (b) **TpPa@IEF-50**, (c) **TpPa@IEF-100**, and (d) **TpPa@IEF-150**, and TEM images of (e) **TpPa-1** and (f) **TpPa@IEF-100**.

(XPS) measurements. Through full spectrum scanning (Fig. S12†), the binding energies of the C, N, Ti and O elements were determined to be 283.0 eV, 398.0 eV, 457.0 eV and 530 eV, respectively. The high-resolution XPS spectrum of C 1s is shown in Fig. 3a, where the binding energies of 283.14 eV, 287.15 eV and 284.8 eV correspond to the characteristic peaks of C=N, C–N and C=C bonds, respectively. As shown in Fig. 3b, the high-resolution spectrum of N 1s indicates that the characteristic peak (398.23 eV) is due to the C=N bond and the peak with a binding energy of 399.86 eV is derived from

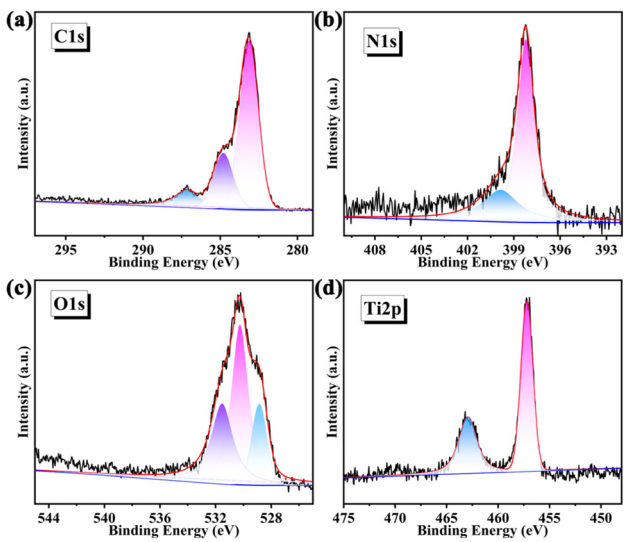

Fig. 3 High-resolution XPS energy spectra of **TpPa@IEF-150**: (a) C 1s, (b) N 1s, (c) O 1s, and (d) Ti 2p.

the C–N bond (Fig. 3b). The binding energy of 530.25 eV in the high-resolution spectrum of O 1s corresponds to the characteristic peak of the Ti–O bond, while the characteristic peak at the binding energy of 531.53 eV is attributed to the C=O bonds of **IEF-11** (Fig. 3c). The high-resolution spectrum of Ti 2p shows the existence of binding energies of 457.20 eV and 462.94 eV, corresponding to the two characteristic peaks of Ti $2p_{3/2}$ and Ti $2p_{1/2}$ (Fig. 3d), respectively.

The CO_2 adsorption curves of **TpPa-1**, **IEF-11** and **TpPa@IEF-*X*** samples are recorded at room temperature. The calculated results show that the CO_2 adsorption capacities of **IEF-11**, **TpPa@IEF-50**, **TpPa@IEF-100**, **TpPa@IEF-150** and **TpPa-1** increased sequentially, corresponding to 9.16 $cm^3\ g^{-1}$, 24.32 $cm^3\ g^{-1}$, 26.84 $cm^3\ g^{-1}$, 29.06 $cm^3\ g^{-1}$ and 42.44 $cm^3\ g^{-1}$, respectively (Fig. S13†). Therefore, the composite photocatalysts **TpPa@IEF-*X*** inherit the adsorption ability of **TpPa-1** toward the substrate CO_2, and the introduction of **TpPa-1** could be beneficial for the CO_2 photocatalytic reduction reaction. To evaluate the light absorption capacity of the catalyst, their optical absorption ability was investigated by UV-vis diffuse reflectance spectroscopy (DRS). The absorption edge of **IEF-11** locates at about 570 nm, which is narrower than that of **TpPa-1**. The optical absorption edges of the hybrid materials **TpPa@IEF-*X*** are similar to that of **TpPa-1** and red-shifted (approximately 630 nm) compared to that of **IEF-11** (Fig. 4a). The composite photocatalysts **TpPa@IEF-*X*** inherit the excellent light capture ability of **TpPa-1** and can achieve a light absorption range similar to that of **TpPa-1**. Through analyzing the DRS spectra, the correlation band gaps with the values of 2.37 eV and 2.14 eV have been calculated for **IEF-11** and **TpPa-1** with the help of the K–M formula, respectively (Fig. 4b). Furthermore, the band structures of **IEF-11** and **TpPa-1** could be established with assistance from the Mott–Schottky (M–S) experiment. The flat band potentials of **IEF-11** (Fig. S14†) and **TpPa-1** (Fig. S15†) are −1.08 eV and −0.81 eV *vs.* the Ag/AgCl electrode, corresponding to −0.88 eV and −0.61 eV (*vs.* NHE), respectively, according to the M–S plots. Based on the positive slope in the M–S plots of **IEF-11** and **TpPa-1**, it is concluded that both of them are n-type semiconductors. Naturally, the conduction bands of **IEF-11** and **TpPa-1** are determined to be −1.08 eV and −0.81 eV, respectively. Naturally, their valence bands are further calculated to be 1.29 eV (**IEF-11**) and 1.33 eV (**TpPa-1**), respectively, based on the energy band relationship.

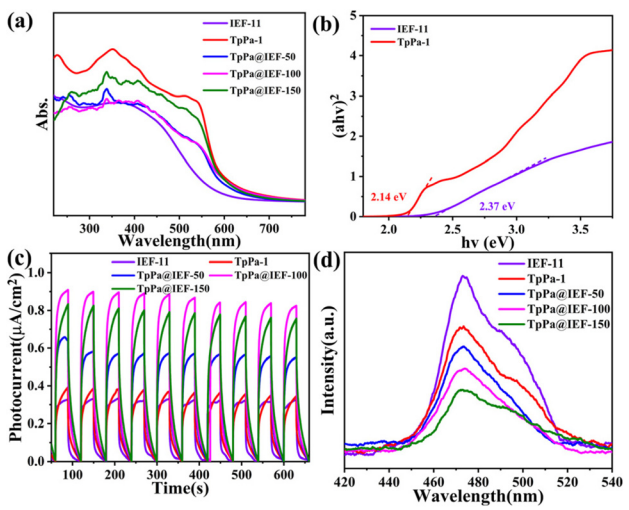

Fig. 4 (a) UV-vis absorption spectra of **IEF-11**, **TpPa-1** and **TpPa@IEF-*X***; (b) band gaps of **IEF-11** and **TpPa-1**; (c) transient photocurrent response graphs of **TpPa-1**, **IEF-11** and **TpPa@IEF-*X***; and (d) photoluminescence spectra of **TpPa-1** and **TpPa@IEF-*X***.

With the help of photoelectrochemical tests, the synthesized photocatalytic materials **TpPa@IEF-*X*** are characterized for their photoelectrochemical properties. The photoluminescence (PL) spectrum is employed to evaluate the recombination rates of photo-generated electron and hole pairs.

The PL intensities of **TpPa-1** and **IEF-11** are significantly higher than those of the hybrid material **TpPa@IEF-*X***, and the PL intensities of **TpPa@IEF-150**, **TpPa@IEF-100** and **TpPa@IEF-50** decrease sequentially (Fig. 4d), which proves that the introduction of **IEF-11** effectively reduces the recombination of photogenerated carriers in the hybrid materials **TpPa@IEF-*X*** and the photoluminescence process is suppressed, providing more photogenerated electrons for the photocatalytic reduction of CO_2. In addition, transient photocurrent response tests further reveal the ability of the sample to separate photogenerated electrons and holes. The transient photocurrent response shows that the photocurrent density of the hybrid materials **TpPa@IEF-*X*** is much higher than those of the original **TpPa-1** and **IEF-11**, demonstrating that the introduction of **IEF-11** indeed improves the separation efficiency of photogenerated electrons and holes. In the electrochemical impedance spectrum, the composite photocatalysts **TpPa@IEF-*X*** exhibit a smaller Nyquist semicircle radius compared to **TpPa-1** and **IEF-11**, which indicates that **TpPa@IEF-*X*** have faster interfacial charge transfer rates (Fig. S16†).

Under the illumination of an LED light source, the homemade photocatalytic reactor was filled with different concentrations of CO_2 gas and a few drops of water to conduct the photocatalytic CO_2 reduction reaction experiment. The photocatalytic reduction procedure is a more advanced gas–solid reaction with water as the reducing agent under the condition of no photosensitizer and sacrificial agent, where the main product is CO as well as a little H_2. The results of the photocatalytic reduction of CO_2 show that the prepared photocatalysts display high selectivity, in which **TpPa@IEF-*X*** possess >90% selectivity (Table S1†). The CO generation rates of these composites **TpPa@IEF-50**, **TpPa@IEF-100** and **TpPa@IEF-150** are 46.48 μmol $g^{-1}\ h^{-1}$, 78.87 μmol $g^{-1}\ h^{-1}$ and 57.61 μmol $g^{-1}\ h^{-1}$, respectively, and their CO generation rates increase by 2.14, 3.63, and 2.65 times, compared to that of **TpPa-1**. It can be seen that the photocatalytic activity of **TpPa@IEF-*X*** in a pure CO_2 environment is higher than those of **TpPa-1** (21.72 μmol $g^{-1}\ h^{-1}$) and **IEF-11** (17.84 μmol $g^{-1}\ h^{-1}$) (Fig. 5a). Moreover, a controlled experiment was also carried out. The photocatalytic capability of the physical mixture based on

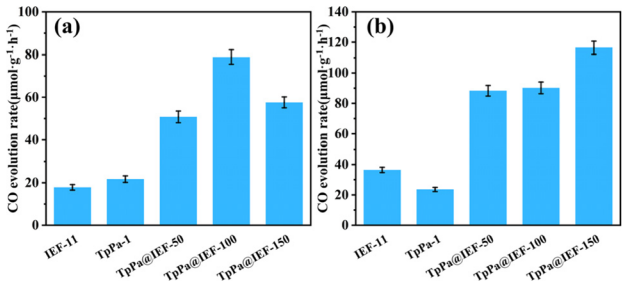

Fig. 5 CO formation rates (a) in a pure CO_2 environment and (b) in a 10% CO_2 environment.

TpPa-1 and **IEF-11** was evaluated, and it should be mentioned that its photocatalytic performance is lower than that of the hybrid materials **TpPa@IEF-*X***. Additionally, the formation rates of CO by **TpPa@IEF-100** at certain times are shown in Fig. S17.† Notably, the same photocatalytic CO_2 reduction experiment was also performed under solar illumination, and the formation rate of CO by **TpPa@IEF-100** was only 1.57 μmol g^{-1} h^{-1}. Therefore, to determine the key factors in the photocatalytic CO_2 conversion process, a series of controlled experiments was conducted. When the steps of the CO_2 reduction reaction are taken in the dark, the reaction system is completely inactive and no products are produced. If the photocatalyst is removed, only water and CO_2 are present in the reaction system, and no products appear. When replacing CO_2 in the reaction system with N_2, the photocatalytic reaction is performed under the same test conditions, and no reaction products are detected, indicating that the generated CO indeed results from the introduced CO_2.

Nowadays, the concentration of CO_2 in anthropogenic emissions from thermal power plants and flue gases is relatively low.[39] Therefore, there is an urgent need to convert CO_2 into useful chemicals at low concentrations because the uptake and activation of CO_2 at low concentrations are very difficult.[40] Although photocatalysts exhibit superior activity in pure CO_2, it is a huge challenge to the continue good catalytic performance at low CO_2 concentrations. Based on this background, the photocatalytic performances of samples are evaluated in a dilute CO_2 gas (10% CO_2 and 90% N_2) environment. It is surprising that **TpPa@IEF-*X*** hybrid materials show excellent photocatalytic performances with high product selectivity (>90% Table S1†). The CO generation rates of **TpPa@IEF-50**, **TpPa@IEF-100** and **TpPa@IEF-150** are 88.32 μmol g^{-1} h^{-1}, 90.21 μmol g^{-1} h^{-1} and 116.47 μmol g^{-1} h^{-1}, respectively (Fig. 5b). **TpPa@IEF** exhibit excellent photocatalytic performances in both pure CO_2 and dilute CO_2 (10%) environments. It should be mentioned that the O_2 generation rates of the composite samples were also calculated, as given in Fig. S18 and S19.† Subsequently, two samples, **TpPa@IEF-100** and **TpPa@IEF-150**, were selected to test the durability of photocatalytic CO_2 reduction, and the samples were still able to maintain high catalytic activity after four cycles of testing (Fig. S20 and S21†). Notably, the photocatalytic effect in the dilute CO_2 (10%) environment is superior compared to that in the pure CO_2 system due to the advantage of CO_2 enrichment resulting from –OH in **TpPa-1**,[41] which allows the photocatalytic reduction of the CO_2 reaction to proceed fully, resulting in an excellent photocatalytic effect. In summary, the prepared photocatalysts surpass the catalytic activity of the parent **TpPa-1** and **IEF-11** in pure CO_2 and dilute CO_2 (10%) environments. Driven by visible light, **TpPa@IEF** provide a constant source of energy for the occurrence of photocatalytic reduction reaction with their excellent light absorption ability, and the reasonable combination can effectively separate and transfer photogenerated charges, thus improving the conversion efficiency of CO_2 into CO. Up to now, **TpPa@IEF** has outperformed some other heterogeneous photocatalysts. Table S2† summarizes and shows the results of the studies on the reduction of CO_2 to CH_4 or CO using COF and its composites as photocatalysts. Compared with the published research results, the photocatalysts **TpPa@IEF** obtain good CO yields using water as the reducing agent in the CO_2 photoreduction process without adding any additives.

The photocatalytic reaction mechanism

A possible mechanism for the photoreduction of CO_2 is presented based on the synergistic effect of **TpPa-1** and **IEF-11** (Fig. 6). Because after photoexcitation, the photogenerated electrons of **IEF-11** leap from the VB to the CB, and then transfer to **TpPa-1** for reducing CO_2. The ordered arrangement of Ti–O–Ti bonds in **IEF-11** is beneficial for carrier transport. The large specific surface area, abundant catalytically active sites and good CO_2 capture ability of **TpPa@IEF-*X*** provide sufficient conditions for photocatalytic CO_2 reduction. Under the irradiation of solar light, the photogenerated CB of **TpPa-1** converts CO_2 into CO, and the remaining holes of **IEF-11** are consumed by H_2O in the reaction system. In the type-II hetero-

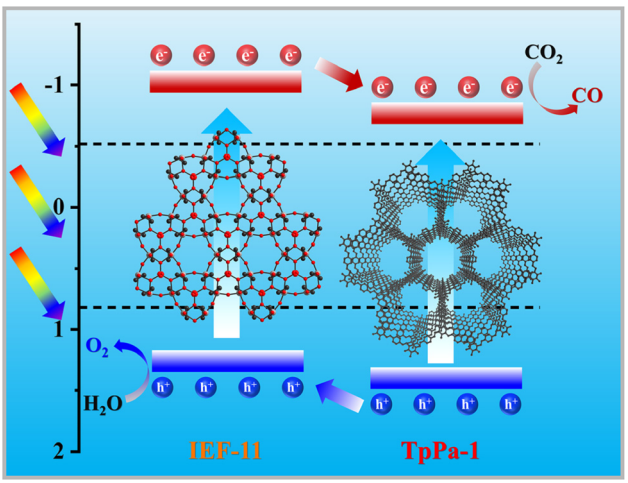

Fig. 6 The mechanism of CO_2 photoreduction by TpPa@IEF-*X*.

junction formed by **TpPa-1** and **IEF-11**, the reverse migration of photogenerated electrons and holes achieves effective separation and promotes the photocatalytic CO_2 reduction reaction.

Conclusions

In summary, a series of stable hybrid materials **TpPa@IEF-*X*** based on **TpPa-1** and **IEF-11** have been prepared and employed for achieving a visible light-driven, sacrificial agent-free and photosensitizer-free photoreduction of CO_2 *via* the gas–solid reaction mode, where **TpPa@IEF-100** achieves great CO formation (78.87 μmol g^{-1} h^{-1}) in a pure CO_2 environment, and **TpPa@IEF-150** obtains an excellent CO generation rate of up to 116.47 μmol g^{-1} h^{-1} in a dilute CO_2 environment. The photochemical measurements show that the rational coupling of **TpPa-1** and **IEF-11** has the natural advantage of broad light absorption ability, rich active sites and efficient photogenerated electron and hole pair separation, finally improving the photoreduction performance of CO_2. This work provides an effective strategy for the preparation of new high-performance photocatalysts, indicating that COF@MOF hybrid materials have promising applications in solar-driven photocatalytic CO_2 reduction systems.

Conflicts of interest

There are no conflicts to declare.

Acknowledgements

This work was financially supported by the Natural Science Foundation of Shandong Province (No. ZR2021MB005 and ZR2021MB074) and the National Natural Science Foundation of China (No. 52176193).

References

1 E. Gong, S. Ali, C. B. Hiragond, H. S. Kim, N. S. Powar, D. Kim, H. Kim and S.-I. In, Solar fuels: Research and development strategies to accelerate photocatalytic CO_2 conversion into hydrocarbon fuels, *Energy Environ. Sci.*, 2022, **15**, 880–937.

2 S. C. Shit, I. Shown, R. Paul, K.-H. Chen, J. Mondal and L.-C. Chen, Integrated nano-architectured photocatalysts for photochemical CO_2 reduction, *Nanoscale*, 2020, **12**, 23301–23332.

3 F. Gong, H. Zhu, Y. Zhang and Y. Li, Biological carbon fixation: From natural to synthetic, *J. CO2 Util.*, 2018, **28**, 221–227.

4 P. Gupta, M. T. Noori, A. E. Núñez and N. Verma, An insight into the bioelectrochemical photoreduction of CO_2 to value-added chemicals, *iScience*, 2021, **24**, 102294.

5 J. Wei, R. Yao, Y. Han, Q. Ge and J. Sun, Towards the development of the emerging process of CO_2 heterogenous hydrogenation into high-value unsaturated heavy hydrocarbons, *Chem. Soc. Rev.*, 2021, **50**, 10764–10805.

6 G. Wang, J. Chen, Y. Ding, P. Cai, L. Yi, Y. Li, C. Tu, Y. Hou, Z. Wen and L. Dai, Electrocatalysis for CO_2 conversion: From fundamentals to value-added products, *Chem. Soc. Rev.*, 2021, **50**, 4993–5061.

7 S. Das, J. Pérez-Ramírez, J. Gong, N. Dewangan, K. Hidajat, B. C. Gates and S. Kawi, Core–shell structured catalysts for thermocatalytic, photocatalytic, and electrocatalytic conversion of CO_2, *Chem. Soc. Rev.*, 2020, **49**, 2937–3004.

8 M. Lu, M. Zhang, J. Liu, Y. Chen, J.-P. Liao, M.-Y. Yang, Y.-P. Cai, S.-L. Li and Y.-Q. Lan, Covalent organic framework based functional materials: important catalysts for efficient CO_2 utilization, *Angew. Chem., Int. Ed.*, 2022, **61**, e202200003.

9 S. Mallakpour, E. Azadi and C. M. Hussain, Emerging new-generation hybrids based on covalent organic frameworks for industrial applications, *New J. Chem.*, 2021, **45**, 7014–7046.

10 F.-M. Zhang, J.-L. Sheng, Z.-D. Yang, X.-J. Sun, H.-L. Tang, M. Lu, H. Dong, F.-C. Shen, J. Liu and Y.-Q. Lan, Rational design of MOF/COF hybrid materials for photocatalytic H_2 evolution in the presence of sacrificial electron donors, *Angew. Chem., Int. Ed.*, 2018, **57**, 12106–12110.

11 L. Stegbauer, K. Schwinghammer and B. V. Lotsch, A hydrazone-based covalent organic framework for photocatalytic hydrogen production, *Chem. Sci.*, 2014, **5**, 2789–2793.

12 J.-X. Cui, L.-J. Wang, L. Feng, B. Meng, Z.-Y. Zhou, Z.-M. Su, K. Wang and S. Liu, A metal-free covalent organic framework as a photocatalyst for CO_2 reduction at low CO_2 concentration in a gas–solid system, *J. Mater. Chem. A*, 2021, **9**, 24895–24902.

13 A. T. Partho, M. Tahir and B. Tahir, Recent advances in covalent organic framework (COF) nanotextures with band engineering for stimulating solar hydrogen production: A comprehensive review, *Int. J. Hydrogen Energy*, 2022, **47**, 34323–34375.

14 C. Xia, K. O. Kirlikovali, T. H. C. Nguyen, X. C. Nguyen, Q. B. Tran, M. K. Duong, M. T. Nguyen Dinh, D. L. T. Nguyen, P. Singh, P. Raizada, V.-H. Nguyen, S. Y. Kim, L. Singh, C. C. Nguyen, M. Shokouhimehr and Q. V. Le, The emerging covalent organic frameworks (COFs) for solar-driven fuels production, *Coord. Chem. Rev.*, 2021, **446**, 214117.

15 R. Shah, S. Ali, F. Raziq, S. Ali, P. M. Ismail, S. Shah, R. Iqbal, X. Wu, W. He, X. Zu, A. Zada, Adnan, F. Mabood, A. Vinu, S. H. Jhung, J. Yi and L. Qiao, Exploration of metal organic frameworks and covalent organic frameworks for energy-related applications, *Coord. Chem. Rev.*, 2023, **477**, 214968.

16 M.-Y. Gao, C.-C. Li, H.-L. Tang, X.-J. Sun, H. Dong and F.-M. Zhang, Boosting visible-light-driven hydrogen evolution of covalent organic frameworks through compositing with MoS_2: A promising candidate for noble-metal-free photocatalysts, *J. Mater. Chem. A*, 2019, **7**, 20193–20200.

17 X. Shi, Y. Yao, Y. Xu, K. Liu, G. Zhu, L. Chi and G. Lu, Imparting catalytic activity to a covalent organic framework material by nanoparticle encapsulation, *ACS Appl. Mater. Interfaces*, 2017, **9**, 7481–7488.
18 Y.-P. Zhang, H.-L. Tang, H. Dong, M.-Y. Gao, C.-C. Li, X.-J. Sun, J.-Z. Wei, Y. Qu, Z.-J. Li and F.-M. Zhang, Covalent-organic framework based Z-scheme heterostructured noble-metal-free photocatalysts for visible-light-driven hydrogen evolution, *J. Mater. Chem. A*, 2020, **8**, 4334–4340.
19 J. Meng, X. Liu, C. Niu, Q. Pang, J. Li, F. Liu, Z. Liu and L. Mai, Advances in metal–organic framework coatings: Versatile synthesis and broad applications, *Chem. Soc. Rev.*, 2020, **49**, 3142–3186.
20 J. Ren, N. M. Musyoka, H. W. Langmi, B. C. North, M. Mathe and X. Kang, Fabrication of core–shell MIL-101 (Cr)@UiO-66(Zr) nanocrystals for hydrogen storage, *Int. J. Hydrogen Energy*, 2014, **39**, 14912–14917.
21 A. Ebadi Amooghin, H. Sanaeepur, R. Luque, H. Garcia and B. Chen, Fluorinated metal–organic frameworks for gas separation, *Chem. Soc. Rev.*, 2022, **51**, 7427–7508.
22 Y. Zheng, S. Zheng, H. Xue and H. Pang, Metal–organic frameworks for lithium–sulfur batteries, *J. Mater. Chem. A*, 2019, **7**, 3469–3491.
23 N. Makhanya, B. Oboirien, J. Ren, N. Musyoka and A. Sciacovelli, Recent advances on thermal energy storage using metal–organic frameworks (MOFs), *J. Energy Storage*, 2021, **34**, 102179.
24 L. Chen, X. Zhang, X. Cheng, Z. Xie, Q. Kuang and L. Zheng, The function of metal–organic frameworks in the application of MOF-based composites, *Nanoscale Adv.*, 2020, **2**, 2628–2647.
25 M. Moharramnejad, A. Ehsani, M. Shahi, S. Gharanli, H. Saremi, R. E. Malekshah, Z. S. Basmenj, S. Salmani and M. Mohammadi, MOF as nanoscale drug delivery devices: Synthesis and recent progress in biomedical applications, *J. Drug Delivery Sci. Technol.*, 2023, **81**, 104285.
26 A. Ahmad, S. Khan, S. Tariq, R. Luque and F. Verpoort, Self-sacrifice MOFs for heterogeneous catalysis: Synthesis mechanisms and future perspectives, *Mater. Today*, 2022, **55**, 137–169.
27 Y. Chen, D. Wang, X. Deng and Z. Li, Metal–organic frameworks (MOFs) for photocatalytic CO_2 reduction, *Catal. Sci. Technol.*, 2017, **7**, 4893–4904.
28 H.-N. Wang, Y.-H. Zou, H.-X. Sun, Y. Chen, S.-L. Li and Y.-Q. Lan, Recent progress and perspectives in heterogeneous photocatalytic CO_2 reduction through a solid-gas mode, *Coord. Chem. Rev.*, 2021, **438**, 213906.
29 M. Tahir, B. Ajiwokewu, A. A. Bankole, O. Ismail, H. Al-Amodi and N. Kumar, MOF based composites with engineering aspects and morphological developments for photocatalytic CO_2 reduction and hydrogen production: A comprehensive review, *J. Environ. Chem. Eng.*, 2023, **11**, 109408.
30 S. Gulati, S. Vijayan, Mansi, S. Kumar, B. Harikumar, M. Trivedi and R. S. Varma, Recent advances in the application of metal–organic frameworks (MOFs)-based nanocatalysts for direct conversion of carbon dioxide (CO_2) to value-added chemicals, *Coord. Chem. Rev.*, 2023, **474**, 214853.
31 S. He, Q. Rong, H. Niu and Y. Cai, Platform for molecular-material dual regulation: A direct Z-scheme MOF/COF heterojunction with enhanced visible-light photocatalytic activity, *Appl. Catal., B*, 2019, **247**, 49–56.
32 H. Assi, G. Mouchaham, N. Steunou, T. Devic and C. Serre, Titanium coordination compounds: From discrete metal complexes to metal–organic frameworks, *Chem. Soc. Rev.*, 2017, **46**, 3431–3452.
33 S.-M. Liu, Z. Zhang, X. Li, H. Jia, M. Ren and S. Liu, Ti-Substituted Keggin-type polyoxotungstate as proton and electron reservoir encaged into metal–organic framework for carbon dioxide photoreduction, *Adv. Mater. Interfaces*, 2018, **5**, 1801062.
34 M. Zhang, J.-N. Chang, Y. Chen, M. Lu, T.-Y. Yu, C. Jiang, S.-L. Li, Y.-P. Cai and Y.-Q. Lan, Controllable synthesis of COFs-based multicomponent nanocomposites from core–shell to yolk-shell and hollow-sphere structure for artificial photosynthesis, *Adv. Mater.*, 2021, **33**, 2105002.
35 C. Guo, F. Duan, S. Zhang, L. He, M. Wang, J. Chen, J. Zhang, Q. Jia, Z. Zhang and M. Du, Heterostructured hybrids of metal–organic frameworks (MOFs) and covalent–organic frameworks (COFs), *J. Mater. Chem. A*, 2022, **10**, 475–507.
36 P. Salcedo-Abraira, A. A. Babaryk, E. Montero-Lanzuela, O. R. Contreras-Almengor, M. Cabrero-Antonino, E. S. Grape, T. Willhammar, S. Navalón, E. Elkäim, H. García and P. Horcajada, A novel porous Ti-squarate as efficient photocatalyst in the overall water splitting reaction under simulated sunlight irradiation, *Adv. Mater.*, 2021, **33**, 2106627.
37 S. Kandambeth, A. Mallick, B. Lukose, M. V. Mane, T. Heine and R. Banerjee, Construction of crystalline 2D covalent organic frameworks with remarkable chemical (acid/base) stability via a combined reversible and irreversible route, *J. Am. Chem. Soc.*, 2012, **134**, 19524–19527.
38 D. Shang, D. Li, B. Chen, B. Luo, Y. Huang and W. Shi, 2D–2D SnS_2/covalent organic framework heterojunction photocatalysts for highly enhanced solar-driven hydrogen evolution without cocatalysts, *ACS Sustainable Chem. Eng.*, 2021, **9**, 14238–14248.
39 K. Li, H. Yu, P. Feron, M. Tade and L. Wardhaugh, Technical and energy performance of an advanced, aqueous ammonia-based CO_2 capture technology for a 500 MW coal-fired power station, *Environ. Sci. Technol.*, 2015, **49**, 10243–10252.
40 G. V. Last and M. T. Schmick, A review of major non-power-related carbon dioxide stream compositions, *Environ. Earth Sci.*, 2015, **74**, 1189–1198.
41 R.-G. Yang, Y.-M. Fu, H.-N. Wang, D.-P. Zhang, Z. Zhou, Y.-Z. Cheng, X. Meng, Y.-O. He and Z.-M. Su, ZIF-8/covalent organic framework for enhanced CO_2 photocatalytic reduction in gas-solid system, *Chem. Eng. J.*, 2022, **450**, 138040.